HELIUM – SELF-INTERSTITIAL ATOM INTERACTION IN FERRITIC ALLOY—L. Ventelon and B. D. Wirth (University of California, Berkeley), C. Domain (Electricite de France)

OBJECTIVE

The objective of this work was to determine the effect of interstitial and substitutional helium atoms on the behavior of self-interstitial atoms and self-interstitial atom clusters in ferritic alloys.

SUMMARY

Atomistic simulations have been performed to investigate the effect of He impurities on the properties and behavior of self-interstitial atom clusters in Fe. Ferritic alloys are candidate fusion energy first wall and breeding blanket structural materials, and will be exposed to high levels of radiation damage and transmutation products in a 14 MeV peaked fusion neutron spectrum. A comparison is made of the interaction energies between interstitial He atoms and a single self-interstitial atom (SIA) obtained with *ab-initio* electronic structure and semi-empirical interatomic potentials using molecular dynamics and conjugate gradient molecular statics calculations. The results provide insight into the validity of semi-empirical interatomic potentials and a basis for extrapolating *ab-initio* results from small to larger system sizes. We also present the results of MD investigation into the migration behavior of SIAs and SIA clusters in the presence of interstitial and substitutional He. The MD simulations reveal a strong interaction between He and SIA clusters, often resulting in SIA – vacancy reactions that spontaneously eject helium into interstitial sites, and provide quantitative information on the interaction radii, trapping – binding energetics and migration behavior of mixed He-SIA clusters.

PROGRESS AND STATUS

Introduction

Associated with the development of long-lived and high-performance fusion materials, one key challenge is dealing with the high-level of helium generated from (n,α) reactions in the first wall and blanket structures. Amongst its harmful consequences, helium has a strong tendency to precipitate into thermally stable helium – vacancy clusters and helium bubbles, which is detrimental to the mechanical properties of metals and alloys [1]. Moreover, helium assists the nucleation and growth of cavities in irradiated materials, leading to swelling [2]. Finally, helium migration and precipitation in the form of grain boundary bubbles can produce high temperature embrittlement. Thus, we are investigating the He diffusion mechanisms in ferritic alloys, including by substitutional and interstitial migration and diffusion by vacancy – helium clusters. Possible reactions that must be incorporated into damage accumulation models of fusion materials performance include trapping/de-trapping interactions with a large number of microstructural defects, including dislocations, grain boundaries, precipitate interfaces, vacancies and self-interstitial atom (SIA) clusters and clustering (precipitation) interactions with vacancy, and possibly even SIA clusters. The primary focus of this work is on the interactions between helium and SIA and SIA clusters.

Interatomic Potentials and Simulation Methods

Atomistic simulations have been performed, using semi-empirical Fe-He potentials, using both molecular dynamics (MD) and molecular statics (MS) methods by conjugate gradients. The Fe-Fe interaction is described by the Ackland version of the Finnis-Sinclair potential [3], which predicts a $\langle 110 \rangle$ dumbbell as the stable self-interstitial atom, with a metastable $\langle 111 \rangle$ dumbbell. The isolated SIA migrates according to this potential by rotation of the $\langle 110 \rangle$ mono-interstitial to the $\langle 111 \rangle$ configuration with an activation energy of about 0.2 eV, followed by a fast migration in the $\langle 111 \rangle$ direction [4]. It is important to note that recent *ab-initio* calculations [5–6] and a semi-empirical potential recently developed for Fe [7], predict a larger energy difference between the $\langle 110 \rangle$ and the $\langle 111 \rangle$ configurations, namely 0.7 eV. However, for larger clusters, the $\langle 111 \rangle$ orientation of the dumbbells within the SIA cluster is energetically preferred for both semi-empirical potentials. Thus, in terms of qualitative analysis of the behavior of SIA and SIA clusters,

the performance of these two potentials are comparable and the use of this new potential will likely only change our quantitative results slightly, but again the focus here is on determining the governing mechanisms which give us insight into material behavior. Such mechanisms likely are much less sensitive to the specific details of the selected interatomic potential. The Fe-He interaction is described by the Wilson and Johnson potential [8], a purely repulsive pair-wise potential. For the He-He interaction, we have used the Beck potential [9], also a semi-empirical pair-wise potential.

Ab-initio calculations have been performed with the Vienna Ab-initio Simulation Package VASP [10–12]. The calculations implement a plane-wave basis set, using pseudo-potential within the PAW formalism to describe the electron-ion interaction. Electron exchange and correlation are described by the Perdew-Zunger functional, adding a non-local correction in the form of the generalised gradient approximation (GGA) of Perdew and Wang. All the calculations were performed with the spin polarised GGA pseudo-potentials from the VASP library. Brillouin zone (BZ) sampling is performed using the Monkhorst-Pack scheme. Point defects as well as pure phases are investigated using the super-cell approach with periodic boundary conditions. The defect calculations are performed at constant volume, thus relaxing only the atomic position in a super-cell dimensioned with the equilibrium lattice parameter for Fe. Calculations with 54 (respectively, 128) atom super-cells are done with a BZ sampling of 125 (respectively, 27) k points and a cut-off energy of 400 eV.

The MD simulations have been performed using a computational box size of $50a_0 \times 50a_0 \times 50a_0$ (containing 250,000 atoms), where a_0 is the Fe lattice parameter, with periodic boundary conditions. The cell size has been systematically varied from $3a_0 \times 3a_0 \times 3a_0$ to $20a_0 \times 20a_0 \times 20a_0$ in the conjugate gradient simulations, using the same interatomic potentials. The conjugate gradient scheme is employed in relaxing the atomic positions, and takes several steps to relax the atoms, allowing the whole relaxation process to be fully automated. Volume relaxation turned out to have a small effect on the binding and formations energies as long as conjugate gradient scheme allows for atomic relaxation around the defect. The MD simulations provide insight into the dynamic mechanisms governing He – point defect interactions, while the static simulations provide the formation and binding energies. For static simulations using semi-empirical potentials and *ab-initio* simulations, we have calculated the binding energy between two entities, A and B, in a bcc iron matrix, containing N atoms as follows. The energy E(N - 1 + A) of a super-cell containing only defect A is added to that E(N - 1 + B) of the super-cell containing only defect B. From this sum, one subtracts the energy E(N - 2 + A + B) of the same super-cell containing A and B interacting, and the reference state (E_{ref}) of the super-cell containing no defect. Thus, $E_b(AB) = [E(N - 1 + A) + E(N - 1 + B)] - [E(N - 2 + A + B) + E_{ref}]$. This method can be extended to three, four and so on entities, as follows:

$$E_b(A_1A_2 \ldots A_n) = \sum_{i=1}^{n} E(A_i) - \left[E(A_1 + A_2 + \ldots + A_n) + (n-1)E_{ref}\right]$$

For substitution energy, the reference state for He is the fcc crystal structure. Details of the calculation methods of the formation and binding energies are described in Ref. [2] for static simulations using semi-empirical potentials, and in Ref. [13] for *ab-initio* simulations.

Results and Discussion

It is believed that helium initially resides in interstitial positions in metallic alloys with a very high mobility [14]. As helium diffuses by an interstitial mechanism in a metal with high vacancy super-saturation, as during irradiation, it will become deeply trapped at a vacancy and the diffusion of the now substitutional helium occurs via a vacancy mechanism. Atomistic simulations within the framework of the multiple frequency diffusion model of Le Claire [15] revealed an effective activation energy of 2.35 eV for thermal helium diffusion and showed that substitutional helium can exchange with a second nearest neighbor vacancy with an activation energy of 0.66 eV [16]. According to the semi-empirical potentials, interstitial He diffuses from octahedral to neighboring octahedral sites with an activation energy of about 0.1 eV, where the migrational saddle point consists of the tetrahedral site. Notably, recent *ab-initio* results show a reversal of the octahedral-tetrahedral site stability, but do reveal similar high mobility (low migrational

activation energy) as an interstitial [6–7]. Further, both this set of semi-empirical potentials and the recent *ab-initio* calculations reveal a strong trapping of substitutional He at vacancies, SIAs and SIA clusters.

The He trapping effect upon SIA clusters has been investigated by both dynamic and static simulations. Figure 1 shows a comparison of the diffusivities of a 20 SIA cluster in pure iron and in the presence of a high concentration of substitutional He. The SIA cluster diffusivity was obtained from MD simulations at 600, 800 and 1000 K in pure Fe and in an Fe alloy containing 2500 atomic parts per million (ppm) of randomly distributed substitutional He. As seen in Fig. 1, the low, practically athermal activation energy of one-dimensional SIA cluster migration changes only slightly as a result of He. This indicates that the fundamental migration mechanism remains the same. However, the diffusivity pre-factor decreases by about one order of magnitude, and indicates that He does slow the net SIA cluster migration. The degree of trapping observed depends on the relative positions of both the He and SIA cluster.

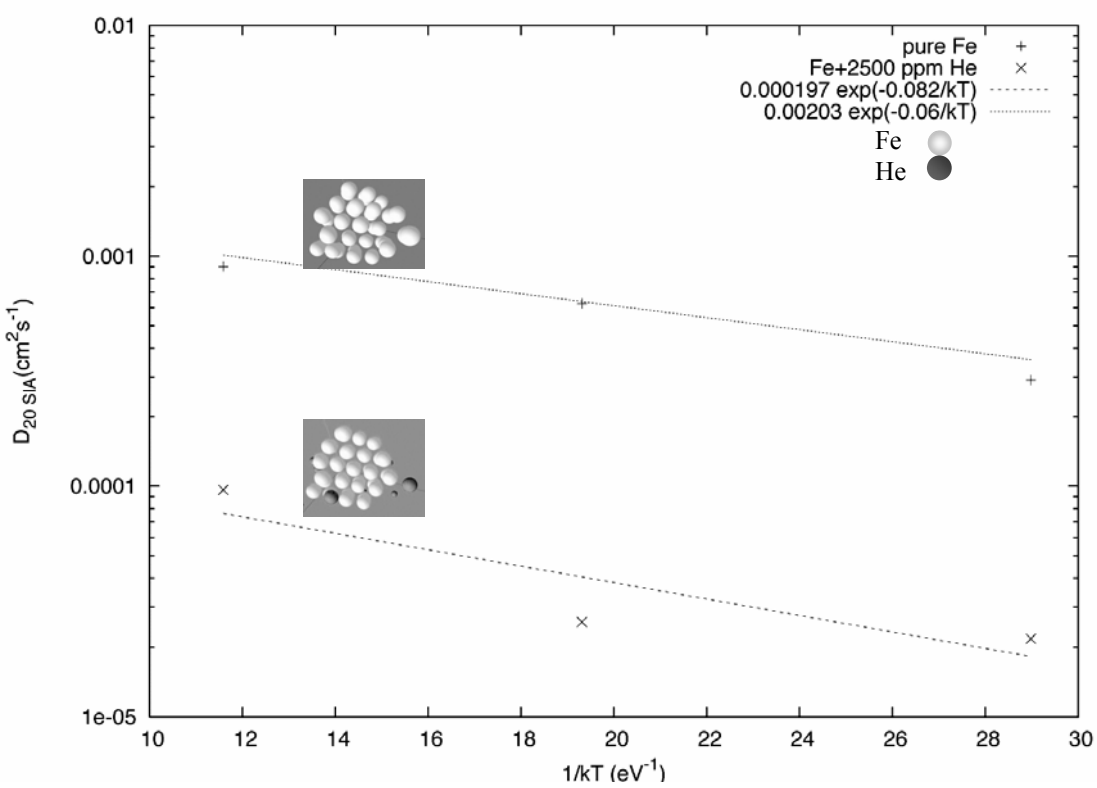

Fig. 1. Comparison of the diffusivities of a 20 SIA cluster in pure iron and in the presence of a high concentration of substitutional He.

Another MD simulation performed at 1000 K in a defected region of otherwise perfect bcc iron containing a high concentration of substitutional He has revealed a large number of interaction phenomena, as shown in Fig. 2. In this figure, a 9 SIA – 2 He cluster, a single vacancy, an isolated SIA, an interstitial He atom and 2 substitutional He atoms from the overall simulation are in close proximity (Fig. 2a). The isolated SIA is about 2.3 nm away from the substitutional He atom. Over several picoseconds, the SIA migrates three-dimensionally with multiple changes of orientation, generally moving towards the nearby helium atom. Upon reaching a separation of about 1.4 nm from the helium in the [111] direction, a fast and spontaneous recombination – replacement reaction occurs (Fig. 2b). In this reaction, the SIA enters the vacant lattice site, recombining with the vacancy and ejecting the helium atom from a substitutional to an interstitial position. The resulting interstitial He rapidly diffuses to and binds with a nearby substitutional He atom for a period of 10 ps, before finally de-trapping (Fig. 2c). Considering the 9 SIA – 2 He cluster, it remains effectively trapped for about 43 ps before the 9 SIA cluster de-traps from the di-He and migrates one-dimensionally towards the isolated vacancy, with which it annihilates (Fig. 2d). Subsequently, the de-

trapped interstitial He migrates to and traps the 8 SIA cluster (Fig. 2e). This simulation has shown a variety of recombination, trapping and de-trapping processes involving He and SIA clusters which merits further study.

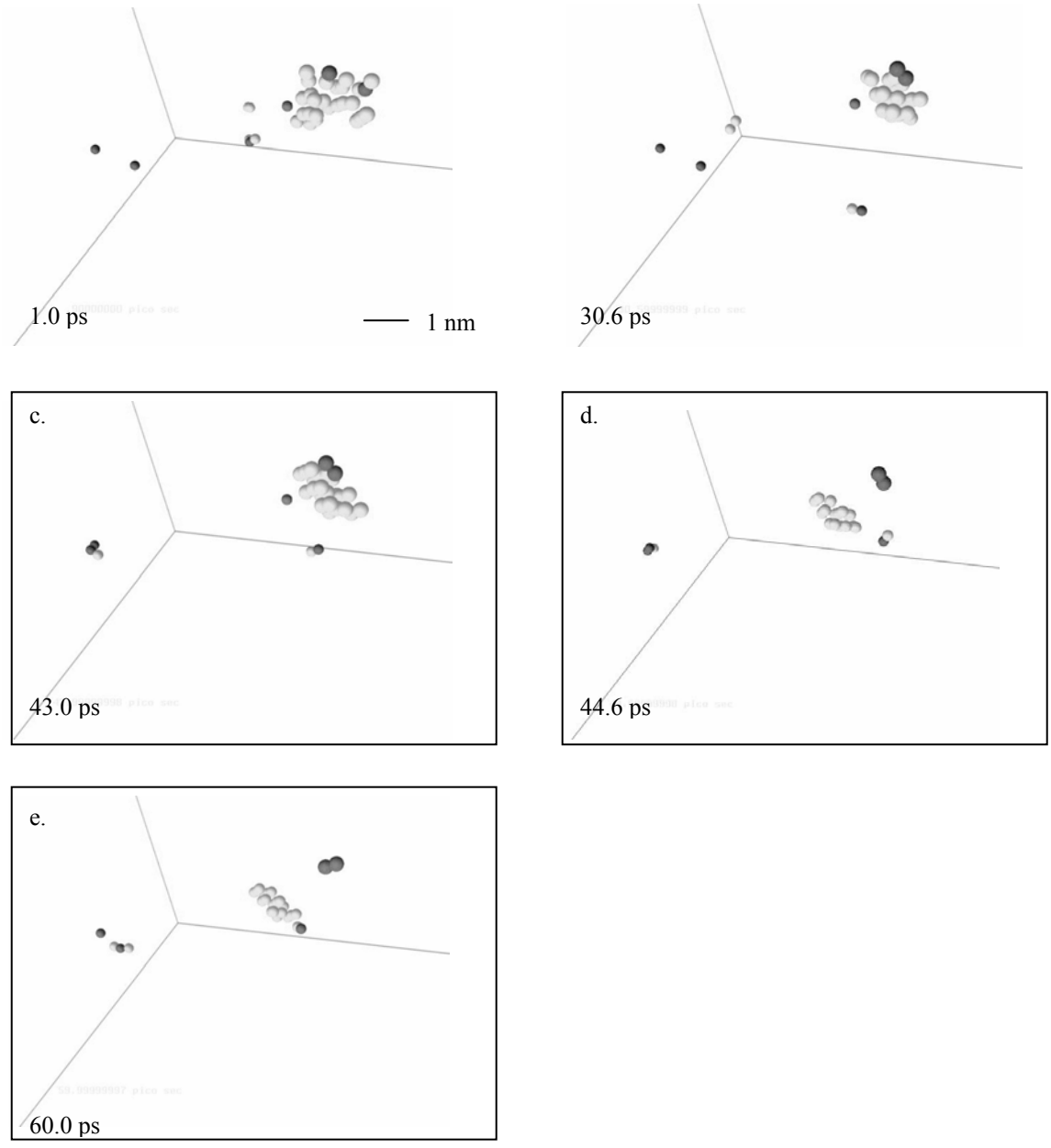

Fig. 2. Series of MD snapshots showing the interaction between SIA and SIA cluster (light gray circles) and neighboring substitutional He atoms (dark gray circles) at 1000K. This simulation shows a fast and spontaneous recombination – replacement reaction (2.a, 2.b), He – He complex formation (2.c), SIA de-trapping from the di-He (2.d) and migration of the de-trapped interstitial He to the SIA cluster (2.e).

Figure 3 shows a series of snapshots in time from an MD simulation at 1000 K showing the interaction between an 11 SIA cluster and 4 substitutional He – 2 vacancy cluster. The 11 SIA cluster, initially about 8 nm away from the He cluster in the [111] direction, migrates one dimensionally along the ⟨111⟩ direction with a net drift towards the He – vacancy cluster (Fig. 3a). When the SIA cluster reaches a separation of about 2 nm from the helium – vacancy cluster, the SIA cluster is spontaneously attracted to the vacancy

cluster complex, where it annihilates (recombines with) the 6 vacant lattice sites and ejects the 4 substitutional He atoms into interstitial positions (Fig. 3b). The SIA cluster and the 4 He interstitial cluster rapidly coalesce to form a 5 SIA – 4 interstitial He cluster (Fig. 3c). The resulting SIA – He cluster is strongly bound and, although the SIA cluster continually attempts to migrate by detaching from the cluster, it is unable to overcome the binding interaction and remains trapped over the time scale of the MD simulation. Notably however, the 5 SIA – 4 interstitial cluster does rotate from its initial ⟨111⟩ direction to a different ⟨111⟩ direction (Fig. 3d).

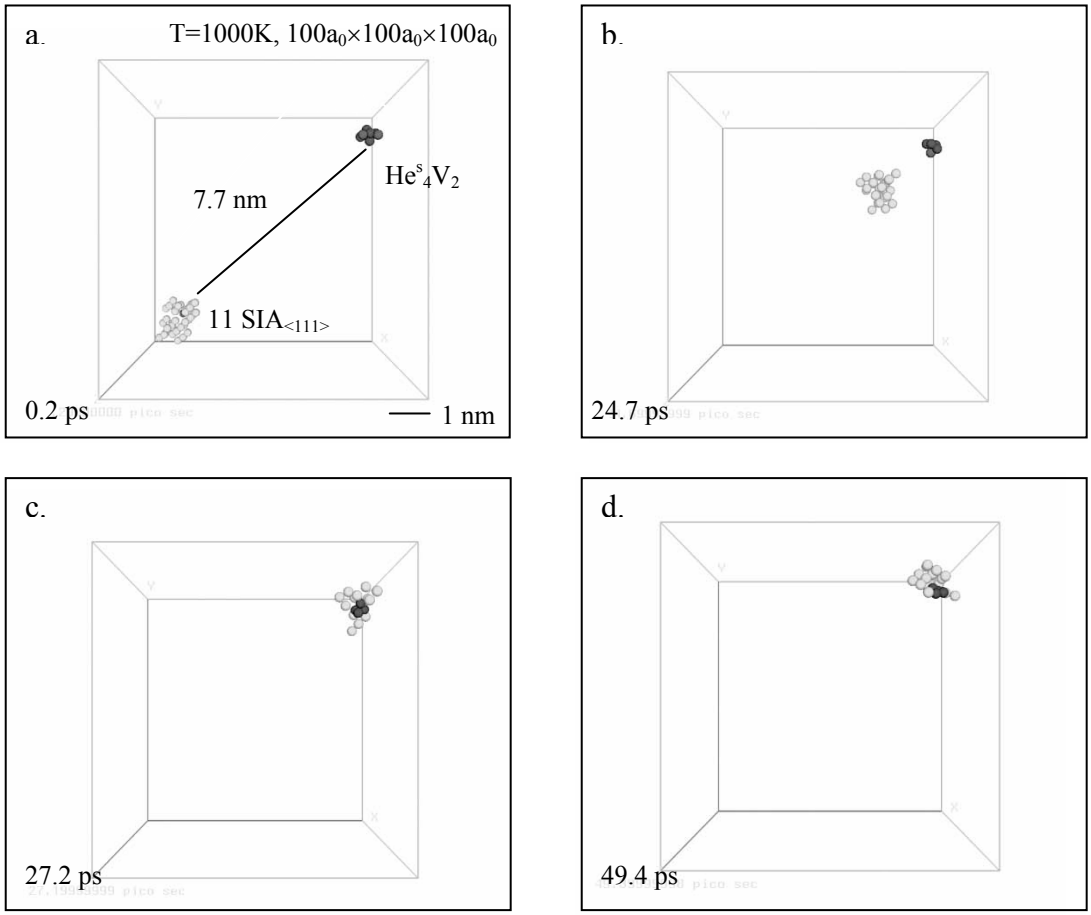

Fig. 3. Series of snapshots from an MD simulation at 1000 K showing the interaction between an 11 SIA cluster (light gray spheres) and 4 substitutional He – 2 vacancy cluster (dark gray spheres). The SIA cluster is spontaneously attracted to the vacancy cluster complex and the resulting SIA – He cluster is strongly bound.

To summarize, our dynamic simulations reveal a long-range interaction between one-dimensionally gliding SIA clusters and substitutional He as well as small He – vacancy clusters, leading to substitutional He – SIA recombination kick-out mechanism that ejects He atoms into interstitial positions. The dynamic simulations also reveal that SIA cluster – He interstitial complexes can be moderately to strongly trapped, depending on the relative size of each cluster. However, the dynamic simulations do not provide the recombination – replacement radii or the trapping – binding energetics. Therefore, we performed molecular statics (MS) calculations using the conjugate gradients method to investigate the energetics of interstitial helium – SIA cluster complexes. The MS results have been interpreted by considering the strain field interactions between the defects. Thus, ⟨111⟩ split interstitial dumbbells, whether isolated or as part of a small SIA cluster loop, have a large anisotropic stress field, compressive along its ⟨111⟩ orientation and tensile along a perpendicular ⟨110⟩ direction. The displacement field of interstitial He is

compressive and roughly spherical. The anticipated stress field interaction between these defects is expected to produce an attractive interaction along the ⟨110⟩ direction perpendicular to the dumbbell(s) orientation and a repulsive interaction along the ⟨111⟩ direction.

Therefore, to provide a quantitative assessment of the binding energy between SIA clusters and interstitial He atom clusters, the He has been displaced along a ⟨110⟩ direction, perpendicular to the ⟨111⟩ orientation of the dumbbells within the cluster. Figure 4 shows the calculated defect energy of a 20 SIA – He^i_1 cluster as a function of the distance between the center of mass of the SIA cluster and of the He atom. Well separated, the pair has a formation energy of 48.11 eV. As the He is moved towards the loop in the conjugate gradient calculations, a slightly positive binding energy of a few hundredths of an eV is obtained. As the He is moved closer to the cluster, a sharp decrease in the total defect energy (increase in binding energy) is observed as the He approaches the loop periphery. The maximum binding energy for He at the loop periphery (distance from center of cluster of approximately 0.5 nm) is 1.25 eV when the He is on a perfect loop ledge, and increases to 1.39 eV when the He is close to the jog point of the loop. Presumably, the increase in binding energy is due to the higher strain energy of the cluster at the jog point. As expected, further motion of the He into the loop interior results in highly negative binding energies. The trapping radius has been assigned by considering the interstitial He trapped when the binding energy exceeds the kinetic energy of the He corresponding to the internal energy of a monoatomic ideal gas, namely when the binding energy is equal to 3/2kT. This is approximately 0.11 eV over the temperature range of 400–700 °C. Notably, especially considering the dynamic simulation results, the interaction or trapping radii obtained from this analysis are quite small, ranging from 0.8 to 1.2 nm, depending on the specific orientation of the interaction between the interstitial helium and the 20-member SIA cluster loop. The relatively strong binding energies of the trapped He^i_1 – 20 SIA complex are large enough to influence microstructural evolution. Assuming that the de-trapping rate is given by a standard Arrhenius form, $k = \nu_o \exp(-(E_b + E_m)/kT)$ where k is the de-trapping rate, E_b the binding energy, E_m the migration energy of the (most) mobile species of about 0.1 eV, with an intrinsic vibrational attempt frequency of 10^{13} s^{-1}, the observed binding energies correspond to mean lifetimes for the trapped complex on the order of 100 ps at 700ºC and 1 μs at 500ºC.

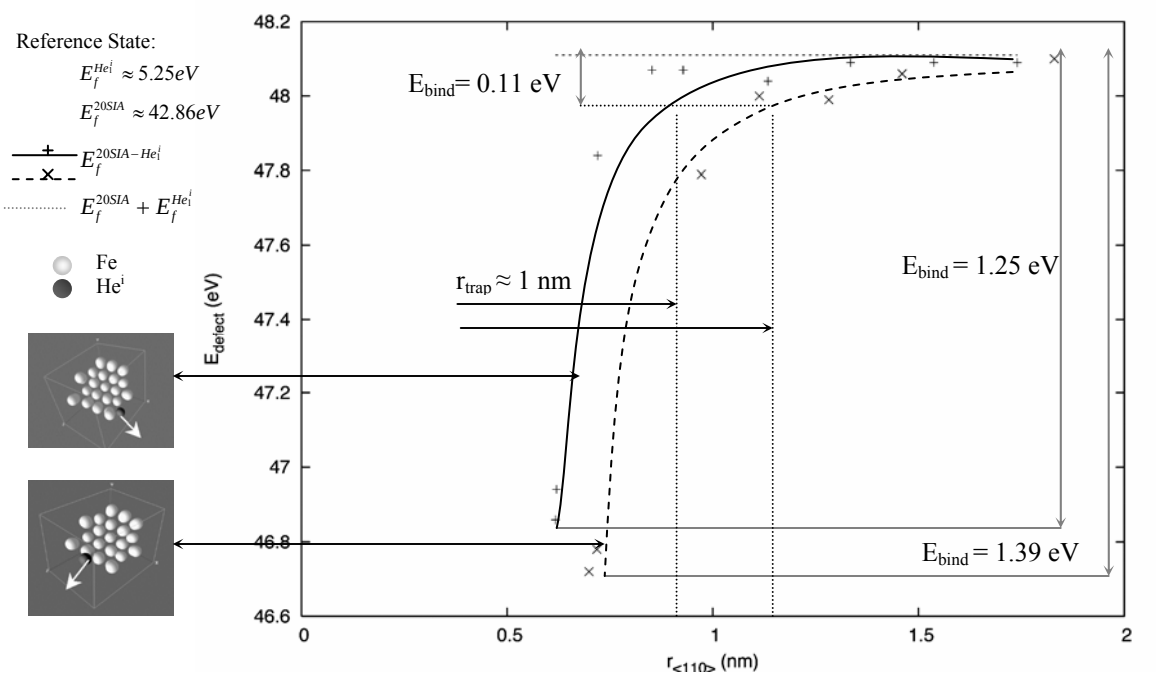

Fig. 4. Calculated defect energy of a 20 SIA – He^i_1 cluster as a function of the distance between the center of mass of the SIA cluster and of the He atom.

Figure 5 shows the results of similar calculations performed for 20 SIA – He^i_2 and – He^i_4 configurations. As expected, the binding energies increase with increasing size of the helium interstitial clusters and depend on the specific geometry of the interaction (e.g., the binding energies are strongest at the loop jog point). The trapping radii are increased slightly over the single interstitial helium but are still quite short, on the order of 1.3 – 1.5 nm. The mean lifetimes calculated at 500 °C for such strongly trapped complexes are on the order of one hour with 2 He atoms and one year with 4 He atoms. These calculations indicate SIA – He^i_n is strongly bound. However, it is again interesting to note that static calculations reveal moderate to high trapping/binding energies, but relatively small interaction/trapping radii. The underlying reasons for the relatively small trapping radii and in particular the apparently smaller values obtained in static vs. dynamic simulations are not known and will require further study. Figure 6 plots the results of our conjugate gradient MS calculations to investigate the binding energies of complexes containing 1, 2, and 4 interstitial helium with 1, 2, 6, 11, and 20 SIA clusters. Although, there is a large amount of scatter in the data, which we believe to result from the specific details of the geometric configurations investigated, the general trends are an increasing binding energy with increasing SIA and He cluster size.

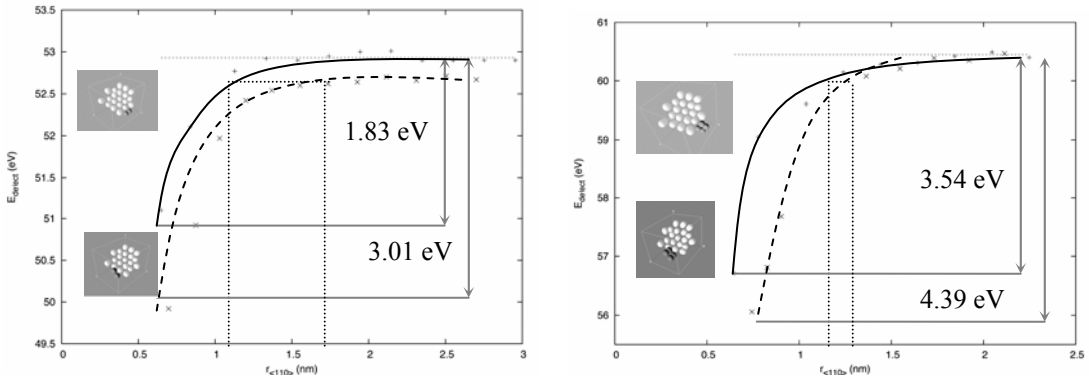

Fig. 5. Similar calculations performed for 20 SIA – He^i_2 and – He^i_4 configurations.

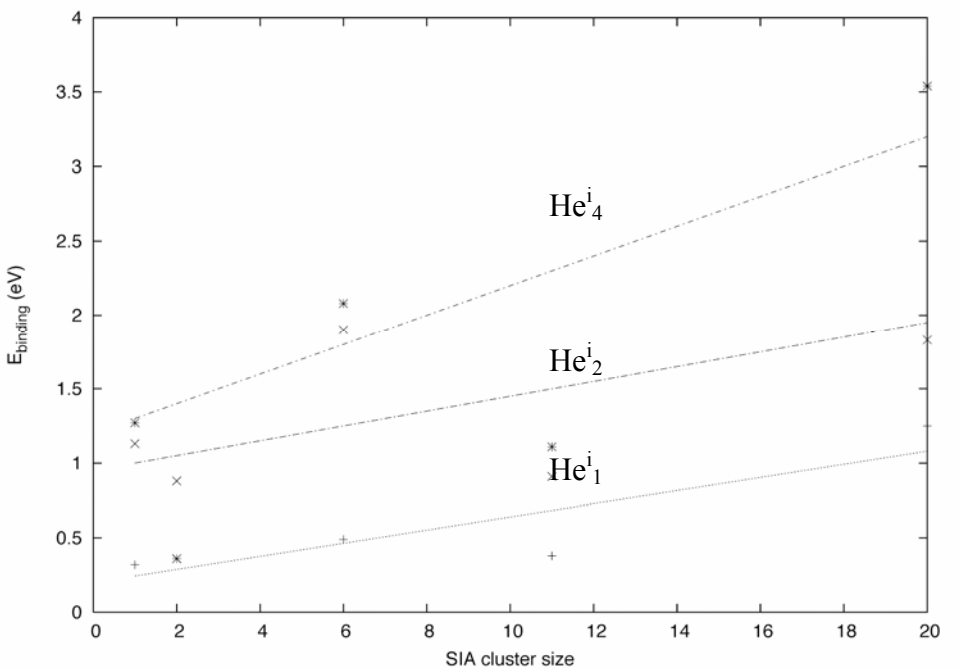

Fig. 6. Conjugate gradient MS calculations investigating the binding energies of complexes containing 1, 2, and 4 interstitial helium with 1, 2, 6, 11, and 20 SIA clusters.

Therefore, we conclude that moderate to strong binding interactions and trapping are expected to occur between SIA/SIA clusters and interstitial He. Surprisingly, the trapping radii governing the interaction are rather small, on the order of 1 nm, and found to be smaller in static than dynamic simulations. We conclude size strain effects are dominant in controlling the strong trapping/binding observed in our simulations.

However, a key question to ask is about the adequacy of the semi-empirical potentials used in this work. Thus, we have compared the interaction energies obtained from our semi-empirical MS simulations to *ab-initio* electronic structure calculations. Besides the previously mentioned reversal in the octahedral-tetrahedral stability of interstitial He in the bcc Fe lattice, the semi-empirical results using a 50×50×50 unit cell are in reasonably good agreement with the VASP calculations performed in a 3×3×3 computational cell, as shown in Table 1.

Table 1. Comparison of formation energies for He – defect configurations between *ab-initio* and semi-empirical potential calculations

Configuration	VASP 54 atoms	Semi-empirical results 250,000 atoms
	He occupation site	
He^s_1	E_f=4.26 eV	E_f=3.25 eV
He^i_1	E_f=4.63 eV E_m=0.2 eV He^i Tetrahedral Octahedral saddle	E_f=5.25 eV E_m=0.1 eV He^i Octahedral Tetrahedral saddle
	He^i_1 - He^i_1 Binding Energy (eV)	
cfg1	0.27	0.43
cfg2	0.38	0.75
	He^i - He^s Binding Energy (eV)	
He^i_1 - He^s_1 ⟨100⟩	1.83	2.18
⟨110⟩	1.91	2.11
He^i_2 - He^s_1	3.62	4.28
He^i_3 - He^s_1	4.97	5.53
He^i_4 - He^s_1	6.62	8.09
He^i_5 - He^s_1	8.38	9.72
	He^s_1 – Vacancy Binding Energy (eV)	
1 nn	0.79	0.33
2 nn	0.51	0.19

The formation energies of substitutional and interstitial He atoms, as well as the binding energies between He atoms are comparable. For both the semi-empirical and *ab-initio* calculations, the interaction (binding) energy between two interstitial He atoms is about 0.5 eV. Although the semi-empirical results give slightly higher binding energies, the two methods predict the same relative stability. In this specific calculation, the interstitial helium pair is on tetrahedral sites in the VASP calculation, whereas the positions have been shifted to octahedral sites for the semi-empirical MS calculation, as shown in Fig. 7. We have also compared the binding energies between a substitutional He atom with one to five neighboring interstitial He atoms. Again, in this case, the interstitial He atoms are inserted on tetrahedral sites using VASP and octahedral sites in the MS calculations. As listed in Table 1, both approaches show the same trend, namely an increasing binding energy with increasing number of interstitial He atoms within the cluster, from about 2 eV up to about 9 eV. Once again, the binding energies obtained from the semi-empirical results are slightly higher than the VASP calculations. We have also compared the energy and configurations of a substitutional He atom with a nearest neighbor vacancy (at either first or second nearest neighbor positions). Both methods predict that the He^s – nearest neighbor complex is energetically preferred and that the He atom prefers to be located away from the lattice site of either vacancy. The VASP results predict stronger binding energy between the substitutional helium – vacancy complex compared to the semi-empirical potential. We conclude from this comparison that the semi-

empirical potentials are performing well in representing helium – point defect interactions, although the quantitative comparison is not quite so favorable.

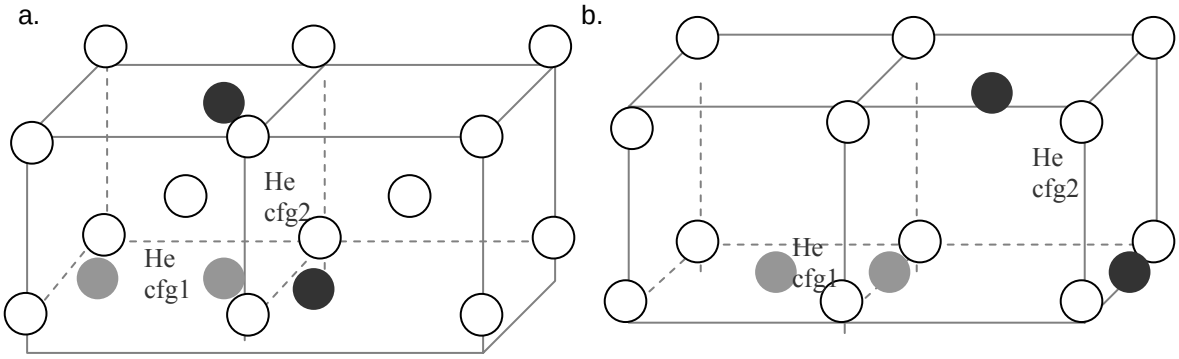

Fig. 7. Interstitial helium pair on tetrahedral sites in the VASP calculation (7.a) and positions shifted to octahedral sites for the semi-empirical MS calculation (7.b).

To complete the comparison, we have considered specifically the binding energy between a ⟨110⟩-oriented Fe SIA and a neighboring interstitial He atom. Three different configurations for the interstitial – self-interstitial atom were used, as shown in Fig. 8. The *ab-initio* calculations were performed with a 54 atom ($3a_0 \times 3a_0 \times 3a_0$) and 128 atom ($4a_0 \times 4a_0 \times 4a_0$) unit cells, while we have performed the semi-empirical MS calculations by systematically varying the cell-size from $3a_0 \times 3a_0 \times 3a_0$ (54 atoms) to $20a_0 \times 20a_0 \times 20a_0$ (250,000 atoms). Table 2 presents the results obtained for computational cell sizes of 54 and 128 atoms. As can be seen, both methods predict configuration 3 to be the most stable, although the semi-empirical potentials predict a change in stability in going from 54 to 128 atoms. However, the absolute agreement between the results presented in Table 2 is not as good as for the previous results presented in Table 1. Perhaps this should not be surprising for situations involving a single SIA, since the *ab-initio* calculations predict a lower formation energy for the ⟨110⟩ split-dumbbell than this semi-empirical potential and a much larger energy difference between the ⟨110⟩- and ⟨111⟩-orientations of the SIA. Moreover, He has been introduced on octahedral sites in the *ab-initio* calculation, even though the preferred configuration for (isolated) interstitial He is the tetrahedral site.

Finally, Fig. 9 presents the results of the size scaling study on the SIA – He interstitial binding energy for each of the three configurations. The results clearly indicate a strong cell-size effect at small cell sizes that does not diminish until larger system sizes on the order of $10a_0 \times 10a_0 \times 10a_0$ are reached. The difference in calculated binding energy for the configurations in increasing the cell size from a $3 \times 3 \times 3$ unit cells to $20 \times 20 \times 20$ is found to be 0.12 ± 0.03 eV, averaged over all three configurations. The major conclusion of the cell-size study is to reinforce that care must be taken in comparing the results of *ab-initio* calculations performed in small super-cells to those of semi-empirical simulations performed at larger size, to properly account for strain field effects due to the periodic images.

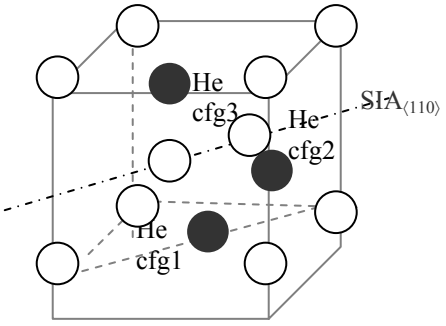

Fig. 8. Three different configurations for the interstitial – self-interstitial atom used for the calculations presented in Table 2.

Table 2. Comparison of *ab-initio* and semi-empirical MS calculations of the SIA – Helium interstitial atom binding energy, as a function of cell size

Configuration	VASP results 54 atoms	VASP results 128 atoms	Semi-empirical results 54 atoms	Semi-empirical results 128 atoms
He^{i}_{1} cfg1	-0.15	-0.09	0.32	0.34
He^{i}_{1} cfg2	-0.04	0.03	-0.15	-0.09
He^{i}_{1} cfg3	0.02	0.07	0.29	0.37

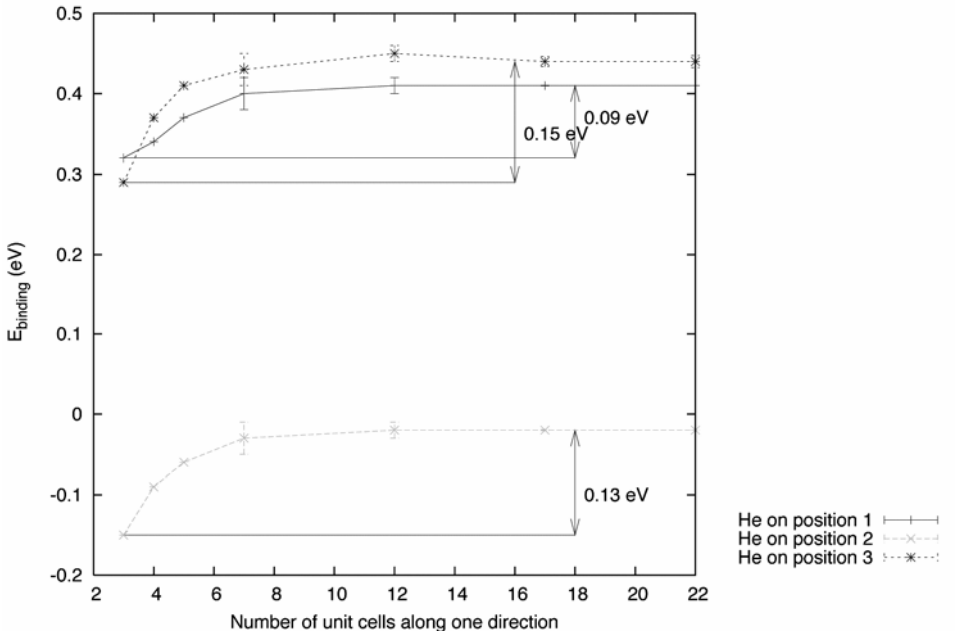

Fig. 9. Size scaling study on the SIA – He interstitial binding energy for each of the three configurations.

Conclusions

The results of atomistic calculations to investigate the effect of He impurities on the properties and behavior of self-interstitial atom clusters in Fe have been presented. The MD simulations using semi-empirical potentials to describe the Fe-He interactions reveal a high mobility of interstitial He in bcc Fe, a strong interaction between interstitial and substitutional He and SIA clusters and a spontaneous SIA – vacancy recombination and kick-out mechanism that ejects the substitutional He into interstitial position.

The MS calculations performed using the conjugate gradient method reveal relatively small interaction radii of about 1 nm between SIA and He cluster complexes, but with strong binding energies from about 1.3 to 4.4 eV. The strong binding interaction between He and SIA clusters effectively traps the otherwise highly mobile SIA clusters for times sufficient to influence the overall microstructural evolution under fusion neutron irradiation conditions. Overall, the results are in good qualitative agreement with *ab-initio* results and indicate that the helium – SIA interactions are governed by size (strain) effects. Future work will seek to clarify some of the issues raised in this study associated with the relatively small interaction radii observed in static vs. dynamic simulations, and will focus on the migration mechanisms and mobility of substitutional helium – vacancy cluster complexes using kinetic Monte Carlo simulations.

Acknowledgements

The authors would like to acknowledge Professor G. Robert Odette (UCSB) and Drs. Takuya Yamamoto (UCSB), Rick Kurtz, Howard Heinisch and Fei Gao (PNNL) and François Willaime and Chu Chun Fu (CEA-Saclay) for many helpful discussions during the course of this work. This work has been supported by the Office of Fusion Energy Sciences, U.S. Department of Energy, under Grant DE-FG02-04ER54750.

References

[1] K. Morishita, R. Sugano, B. D. Wirth, and T. Diaz de la Rubia, Nucl. Instrum. Methods B 202 (2003) 76–81.
[2] K. Morishita, R. Sugano, and B. D. Wirth, J. Nucl. Mater. 323 (2003) 243–250.
[3] G. J. Ackland, D. J. Bacon, A. F. Calder, and T. Harry, Philos. Mag. A 75 (1997) 713.
[4] B. D. Wirth, G. R. Odette, D. Maroudas, and G. E. Lucas, J. Nucl. Mater. 244 (1997) 185.
[5] C. C. Fu, F. Willaime, and P. Ordejón, Phys. Rev. Lett. 92 (2004) 175503.
[6] F. Willaime, C. C. Fu, M. C. Marinica, and J. Dalla Torre, Nucl. Instrum. Methods *B* 228 (2005) 92–99.
[7] M. I. Mendelev, S. Han, D. J. Srolovitz, G. Ackland, D. Y. Sun, and M. Asta, Philos. Mag. 83 (2003) 3977.
[8] W. D. Wilson and R. D. Johnson, In P. C. Gehlen, J. R. Beeler Jr., and R. I. Jaffee (eds.), Interatomic Potentials and Simulation of Lattice Defects, Plenum (1972) 375.
[9] D. E. Beck, Mol. Phys. 14 (1968) 311.
[10] G. Kresse and J. Hafner, Phys. Rev. B 47 (1993) 558.
[11] G. Kresse and J. Hafner, Phys. Rev. B 49 (1994) 14251.
[12] G. Kresse and J. Furthmüller, Comput. Mater. Sci. 6 (1996) 15.
[13] C. Domain, C. S. Becquart, and J. Foct, Phys. Rev. B 69 (2004) 144112.
[14] K. Morishita, B. D. Wirth, T. Diaz de la Rubia, and A. Kimura, In S. Hanada, Z. Zhong, S. W. Nam, and R. N. Wright (eds.), Proceedings of the Fourth Pacific Rim International Conference on Advanced Materials and Processing (PRICM4), The Japan Institute of Metals (2001) 1383.
[15] A. D. Le Claire, J. Nucl. Mater. 69&70 (1978) 70.
[16] B. D. Wirth, G. R. Odette, J. Marian, L. Ventelon, J. A. Young-Vandersall, and L. A. Zepeda-Ruiz, J. Nucl. Mater. 329–333 (2004) 103–111.